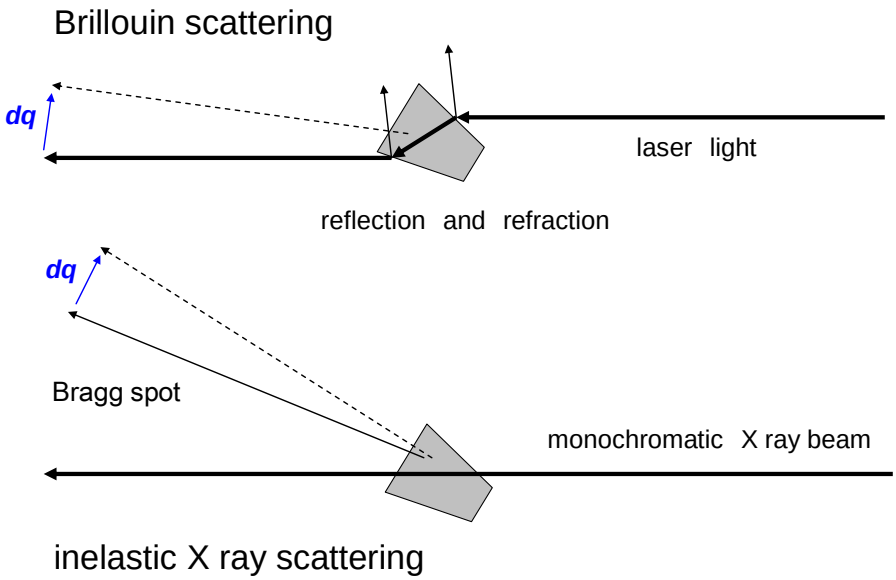

Supplementary Figure 1. Schematic comparison of BS and IXS. The dashed lines are rays scattered in the collision between a phonon and photon in sample (gray tetragons). The vector ***dq*** (blue arrows) shows the momentum change for the photon, which is identical to that for the phonon. The vector specifies not only the magnitude of phonon momentum change but also the propagating direction of the phonon scattered by the X-ray photon.

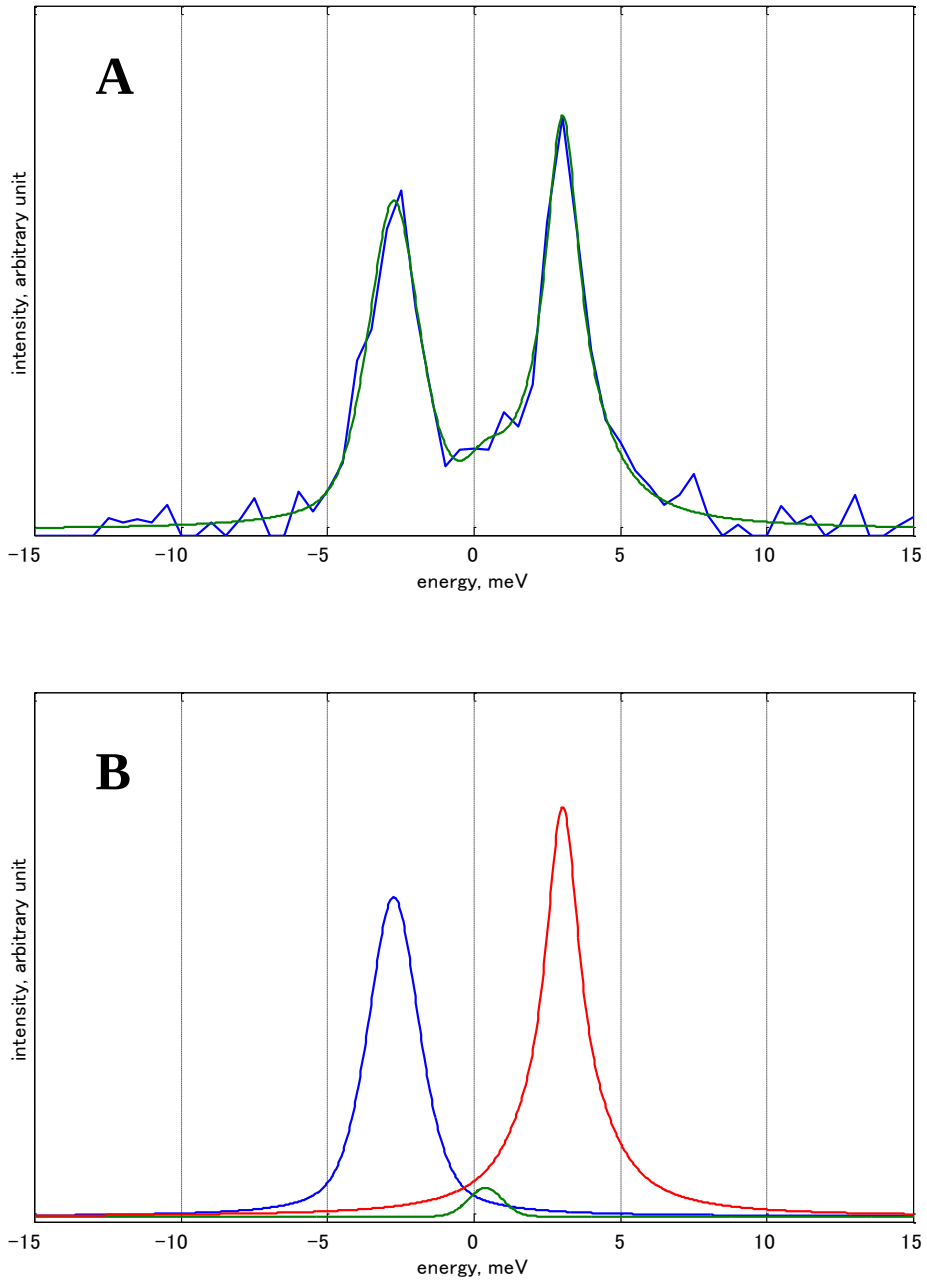

Supplementary Figure 2. An example of IXS peaks. (A) Raw data (blue line) and curve fitted using a pseudo-Voigt function (green line). (B) Decomposed plot for three peaks. The central peak (green line) corresponds to elastic scattering, the right peak to phonon formation, and the left peak to phonon annihilation.

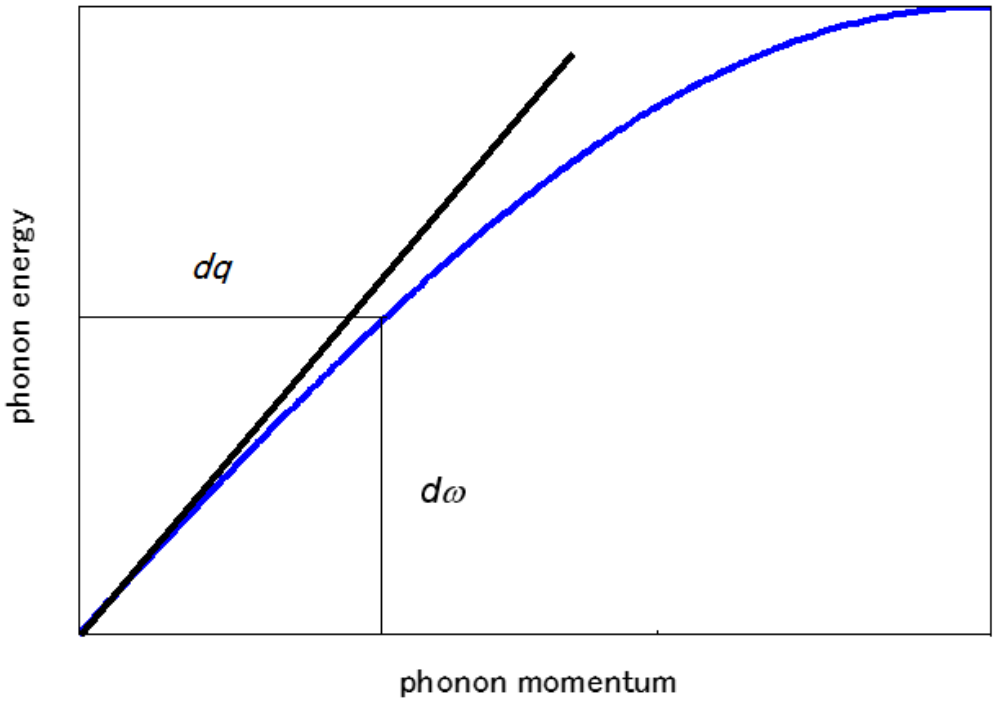

Supplementary Figure 3. Schematic view of the phonon dispersion curve. The left end is the Γ point, where ***dq*** = 0, and the right end is the boundary of the first Brillouin zone. The ratio between observed ***dq*** and $d\omega$ deviates slightly from the initial slope (black line) of the dispersion curve. From the symmetry at the Brillouin zone boundary, the slope at the boundary must be horizontal. In this plot, the blue curve is a quarter-cycle sinusoidal function, which may be the simplest functional form to satisfy the minimum requirements for phonon dispersion.

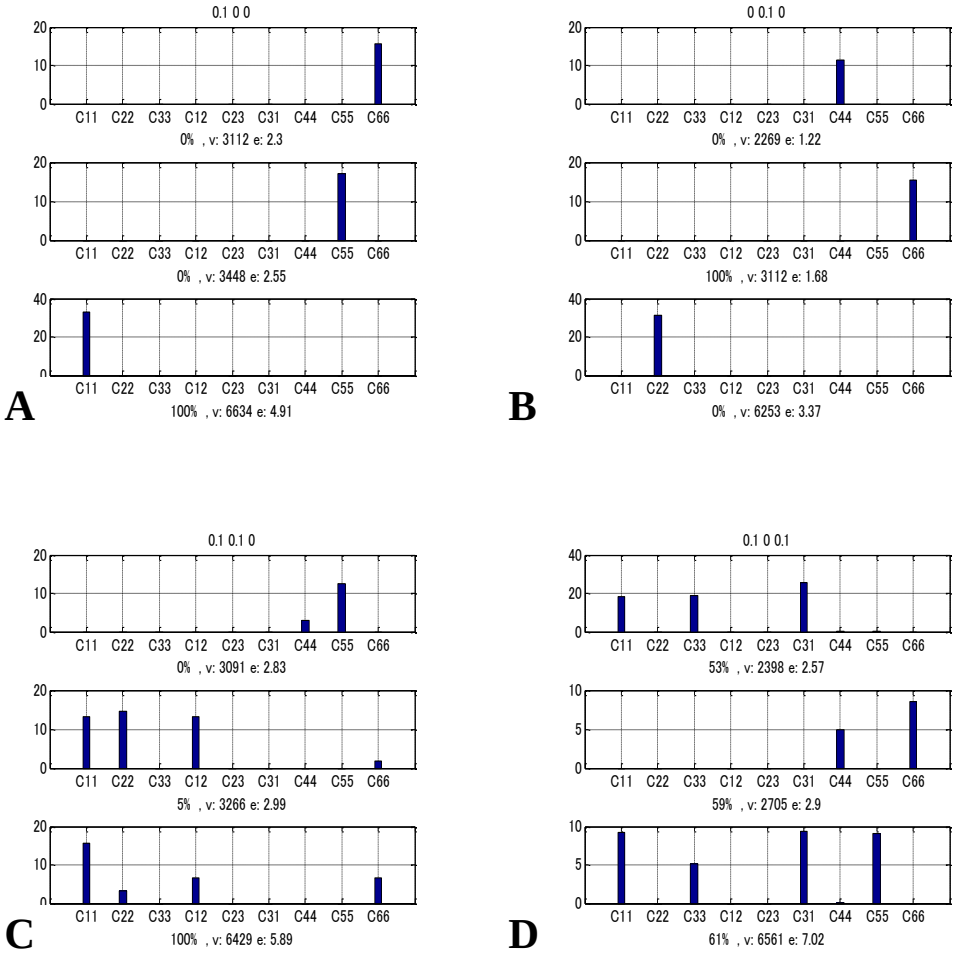

Supplementary Figure 4. Sensitivity pre-analysis of elastic constants. Four examples of pre-analysis for the *Cmcm*-$CaIrO_3$ experiment, showing the sensitivity of each elastic constant to the velocity of the acoustic wave propagating in the direction given by ***dq***. The unit of vertical axes is (m/s)/GPa. (A) ***dq*** = (0.1 0 0) from the Bragg spot of 200. (B) ***dq*** = (0 0.1 0) from the Bragg spot of 200. (C) ***dq*** = (0.1 0.1 0) from the Bragg spot of 220. (D) ***dq*** = (0.1 0 0.1) from the Bragg spot of 220. In each direction, results for the slower S wave, faster S wave, and P wave are shown from top to bottom. The relative intensity (%), velocity (m/s), and energy shift (meV) are given below each plot.

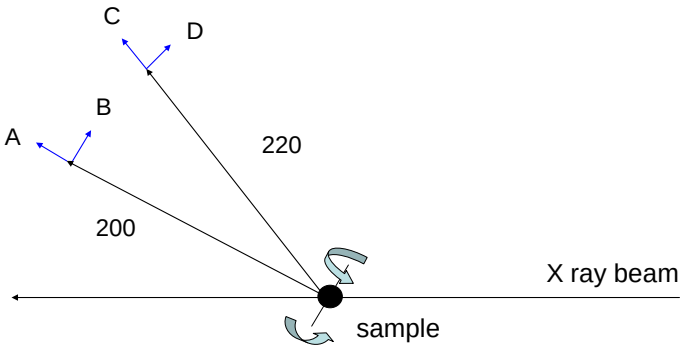

Supplementary Figure 5. Basic configuration of the IXS measurement. Blue arrows correspond to bar graphs with the same label in Supplementary Fig. 4.

Supplementary Table 1. Sound-wave velocities in *Pbnm*-$CaIrO_3$. Each measurement is specified by momentum change, ***dq*** (nm^{-1}), from the Bragg spot. V_{obs} and V_{cal} (km/s) are the observed and calculated velocities; Δ is the percentage difference between them. The mode column specifies the P wave, faster S wave, and slower S wave by 'P', 'FS', and 'SS', respectively. Supplementary Tables 1 and 2 list the detected modes for *Pbnm*-$CaIrO_3$ and *Cmcm*-$CaIrO_3$, respectively. The nine elastic constants were then determined applying least-squares fitting using the Christoffel equation[2].

Data no.	Bragg index			***dq***			V_{obs}	V_{cal}	Δ	mode
1	0	4	0	0.0020	0.2020	0.0160	5.8493	5.8632	0.2	P
2	0	4	0	0.0060	0.1070	0.0480	6.0499	5.9281	-2.0	P
3	0	4	0	0.0940	0.2020	-0.0070	5.8613	5.8806	0.3	P
4	0	4	0	0.0980	0.1070	0.0260	2.6839	2.7601	2.8	SS
5	0	4	0	0.0980	0.1070	0.0260	5.6709	5.8217	2.6	P
6	0	4	0	0.2450	0.0470	-0.0160	2.9398	3.0642	4.2	FS
7	0	4	0	0.2650	-0.1410	0.0510	2.8565	2.8691	0.4	FS
8	0	4	0	0.3370	0.0540	-0.0400	3.1113	3.0799	-1.0	FS
9	0	4	0	0.3470	-0.0410	-0.0070	3.1307	3.0951	-1.1	FS
10	0	4	0	0.3580	-0.1350	0.0280	2.8647	2.9542	3.1	FS
11	0	4	0	0.1530	0.0410	0.0090	3.1638	3.0219	-4.5	FS
12	0	4	0	0.1630	-0.0530	0.0420	2.9816	2.9933	0.4	FS
13	0	4	0	-0.0020	0.0470	0.2310	3.2141	3.2016	-0.4	FS
14	0	4	0	0.0020	-0.0470	0.2700	3.3772	3.2209	-4.6	FS
15	0	4	0	0.0070	-0.1400	0.3100	3.0464	3.0420	- 0.1	FS
16	0	4	0	-0.0940	0.0480	0.2580	3.1742	3.1884	0.4	FS
17	4	0	0	0.2050	-0.0030	0.0160	5.4072	5.3851	-0.4	P
18	4	0	0	0.1140	-0.0110	0.0490	5.4649	5.4098	-1.0	P

19	4	0	0	0.1370	0.3500	-0.0480	2.9354	2.9465	0.4	SS
20	4	0	0	0.0460	0.3500	-0.0160	3.0815	3.0913	0.3	SS
21	4	0	0	-0.0450	0.3500	0.0170	3.0480	3.0923	1.5	SS
22	4	0	0	-0.0530	0.2570	-0.0270	3.2314	3.0567	-5.4	SS
23	4	0	0	0.1440	0.4420	-0.0030	2.9825	2.9918	0.3	SS
24	4	0	0	-0.0380	0.4420	0.0620	3.1374	3.1011	-1.2	SS
25	4	0	0	0.0450	0.0030	0.2300	2.9273	2.7761	-5.2	SS
26	4	0	0	-0.0450	-0.0030	0.2700	2.7082	2.7642	2.1	SS
27	4	0	0	-0.1340	-0.0090	0.3120	2.8799	2.8777	-0.1	SS
28	4	0	0	-0.0440	0.0930	0.3010	2.7206	2.8067	3.2	SS
29	0	0	4	-0.0130	-0.0220	0.1010	5.9417	5.9607	0.3	P
30	0	0	4	0.2010	0.0070	0.0670	2.8785	2.7719	-3.7	SS
31	0	0	4	0.1990	-0.0080	-0.0600	2.6254	2.7649	5.3	SS
32	0	0	4	0.2810	-0.0440	0.0750	2.8100	2.7689	-1.5	SS
33	0	0	4	0.1790	-0.0070	0.1130	2.9080	2.8467	-2.1	SS
34	0	0	4	0.1760	-0.0230	-0.0190	2.7402	2.7421	0.1	SS
35	0	0	4	0.2560	-0.0740	-0.0120	2.7647	2.7717	0.3	SS
36	0	0	4	-0.0940	0.2170	-0.0160	3.0555	3.1944	4.5	FS
37	0	0	4	0.1380	0.1350	0.0730	3.0087	3.0208	0.4	FS
38	0	0	4	0.1520	0.1550	0.1670	2.9454	3.0485	3.5	FS

Supplementary Table 2. Sound-wave velocities in *Cmcm*-$CaIrO_3$. The notation is the same as that in Supplementary Table 1. Supplementary Tables 1 and 2 list the detected modes for *Pbnm*-$CaIrO_3$ and *Cmcm*-$CaIrO_3$, respectively. The nine elastic constants were then determined applying least-squares fitting using the Christoffel equation[2].

Data no.	Bragg index			***dq***			V_{obs}	V_{cal}	Δ	mode
1	0	0	6	0.0010	-0.0240	-0.2040	6.3540	6.6101	4.0	P
2	0	0	4	0.0010	-0.0170	0.2370	6.6846	6.6156	-1.0	P
3	0	0	4	-0.0660	-0.0430	0.2370	5.9023	5.9846	1.4	P
4	0	0	4	-0.0660	-0.0430	0.2370	4.0240	3.9270	-2.4	FS
5	0	0	4	0.0660	0.0400	0.0830	3.7347	3.6919	-1.1	FS
6	0	0	4	0.0680	0.0060	0.2370	5.9358	5.9659	0.5	P
7	0	0	4	0.0740	0.0470	-0.1520	4.0509	4.1868	3.4	FS
8	0	0	4	-0.0760	0.0160	0.0030	2.7049	2.6194	-3.2	SS
9	0	0	4	-0.0780	-0.0170	0.1570	4.3465	4.1878	-3.7	FS
10	0	0	4	-0.0790	-0.0530	0.3110	5.8132	6.0512	4.1	P
11	0	0	4	-0.1430	-0.0100	-0.0040	2.6955	2.6168	-2.9	SS
12	0	0	4	-0.1450	-0.0430	0.1500	3.5169	3.4474	-2.0	FS
13	0	0	4	-0.0110	0.0060	0.1640	6.8734	6.5641	-4.5	P
14	0	4	0	-0.0670	-0.1150	-0.0250	3.2971	3.4206	3.7	FS
15	0	4	0	-0.0670	0.0950	-0.0080	3.5291	3.3526	-5.0	FS
16	2	0	0	0.0210	0	-0.0430	5.5724	5.8546	5.0	P
17	2	0	0	0.0870	0	-0.0150	7.0415	6.7739	-3.8	P
18	2	0	0	0.0210	0.2110	-0.0430	3.4665	3.3645	-2.9	FS
19	2	0	0	0.0870	0.2110	-0.0150	6.3680	6.2147	-2.4	P
20	2	0	0	0.1530	0.2110	0.0150	6.4329	6.5346	1.6	P
21	2	0	0	0.1530	0.2110	0.0150	3.3163	3.3462	0.9	FS
22	2	0	0	0.0870	-0.2110	-0.0130	6.3900	6.2161	-2.7	P
23	2	0	0	0.0870	-0.2110	-0.0130	3.5288	3.4752	-1.5	FS

24	2	0	0	0.1530	-0.2110	0.0170	6.3862	6.5337	2.3	P
25	2	0	0	0.1530	-0.2110	0.0170	3.3726	3.3466	-0.8	FS
26	2	0	0	-0.0710	0.3060	-0.0410	3.4217	3.5399	3.5	FS
27	2	0	0	-0.0040	0.3100	-0.0140	3.1759	3.2101	1.8	FS
28	2	0	0	0.0620	0.3130	0.0150	5.5370	5.7758	4.3	P
29	2	0	0	0.0620	0.3130	0.0150	3.3897	3.4889	2.9	FS
30	2	0	0	-0.0690	-0.1170	-0.0390	3.3174	3.4580	4.2	FS
31	2	0	0	-0.0020	-0.1130	-0.0120	3.0533	3.2050	5.0	FS
32	2	0	0	0.0640	-0.1100	0.0170	6.6784	6.4132	-4.0	FS
33	2	0	0	0.0640	-0.1100	0.0170	3.5112	3.4066	-3.0	FS
34	2	0	0	0.1300	-0.1060	0.0470	6.7317	6.6380	-1.4	P
35	2	2	0	0.1010	0.1020	0.0160	6.8164	6.6328	-2.7	P
36	2	2	0	-0.0450	0.1760	-0.0440	3.4876	3.6173	3.7	FS
37	2	2	0	0.0810	0.3030	0.0150	5.7451	5.9282	3.2	P
38	2	2	0	0.0810	0.3030	0.0150	3.6678	3.5205	-4.0	FS
39	2	2	0	0.1220	-0.1000	0.0180	6.5396	6.6798	2.1	P
40	2	2	0	0.1220	-0.1000	0.0180	3.2254	3.2678	1.3	FS
41	2	2	0	0.1850	-0.0370	0.0500	3.2895	3.2116	-2.4	FS
42	2	0	2	-0.0330	0.0590	-0.0090	3.4364	3.4168	-0.6	FS
43	2	0	2	0.0910	-0.0210	0.0960	6.3737	6.3686	-0.1	P
44	2	0	2	0.1530	-0.0640	0.1480	6.1398	6.4119	4.4	P
45	2	0	2	-0.0590	-0.0040	0.1280	4.0774	4.2294	3.7	FS
46	2	0	2	0.0030	-0.0430	0.1810	2.9256	3.0551	4.4	FS
47	2	0	2	0.0650	-0.0840	0.2330	6.0756	5.9748	-1.7	P
48	2	0	2	0.0650	-0.0840	0.2330	3.8439	3.9124	1.8	FS
49	2	0	2	0.0540	0.0810	-0.0940	5.7485	5.9229	3.0	P
50	2	0	2	0.1170	0.0400	-0.0410	2.6471	2.7422	3.6	SS
51	2	0	2	0.1790	-0.0030	0.0100	2.6197	2.6191	-0.05	SS
52	0	0	4	-0.0680	0.1280	0.0030	2.7506	2.7362	-0.55	SS

53	0	0	4	0.0680	0.1490	0.1570	3.9249	4.0618	3.5	FS
54	0	0	4	0.0010	0.1560	0.1570	6.4909	6.2221	-4.2	P
55	0	0	4	0.0010	0.1870	0.1580	3.2041	3.1541	-1.6	FS
56	0	0	4	-0.0690	0.2100	-0.1520	3.8651	3.9317	1.7	FS
57	0	0	4	-0.0690	0.2100	-0.1520	2.9836	2.9705	-0.4	SS
58	0	0	4	-0.0660	0.1610	0.1580	3.9097	4.0289	3.0	FS
59	0	0	4	0.0650	0.2590	-0.1540	2.9162	2.9491	1.1	SS
60	0	0	4	0.0680	0.2100	0.1570	6.0390	5.8037	-3.9	P
61	0	0	4	0.0680	0.2100	0.1570	4.0600	3.9321	-3.2	FS
62	0	0	4	0.0680	0.2100	0.1570	3.1207	2.9714	-4.8	SS

Supplementary Methods

Supplementary Figure 1 shows the difference between inelastic X-ray scattering (IXS) and Brillouin scattering (BS) mainly from the viewpoint of the geometrical setting[1]. One of the advantages of IXS is that there is more freedom of crystal orientation relative to the incident X-ray beam using Bragg diffraction spots. The other advantage is that IXS is free from reflection and refraction effects, which must be corrected in BS. The vector ***dq*** is the momentum, or wave number, of a phonon colliding with a photon. Note that the direction of ***dq*** is identical to that of the phonon velocity, ***V***. The direction and magnitude of ***dq*** is determined from the geometrical configuration of the detector, sample, and incident X-ray beam.

The velocity of the phonon is determined as

$$V = \frac{d\omega}{|dq|} \quad , \tag{S1}$$

where $d\omega$ is the difference in energy between the scattered X-ray and monochromatic X-ray in terms of angular frequency. The magnitude of $d\omega$ is typically a few meV, which corresponds to 0.1–1 THz. At BL35XU, SPring-8, the 12 (4 × 3)-detector array simultaneously monitors energy change of the scattered X-ray, which is identical to the energy of colliding phonon. Supplementary Figure 2 shows an example of raw measurement data for scattered X-ray photons and the curve fitting procedure using a pseudo-Voigt function to determine peak positions for the energy change of the scattered X-ray.

It is well known that the phonon dispersion curve is notably inflected in that frequency range[1]. We corrected for the phonon dispersion effect by assuming a quarter-cycle sinusoidal function, because the acoustic-wave velocity is defined as the initial slope of the phonon dispersion curve (Supplementary Figure 3). In contrast, this effect does not matter so much in BS, because ***dq*** and $d\omega$ are much smaller (~one-tenth) than values in IXS.

Both *Pbnm*-$CaIrO_3$ and *Cmcm*-$CaIrO_3$ have orthorhombic symmetry and thus have nine independent elastic constants. The diagonal elastic constants (C_{11}, C_{22}, C_{33}, C_{44}, C_{55}, C_{66}) have nearly independent mode propagating crystallographic axes, whereas

the off-diagonal constants (C_{12}, C_{23}, C_{31}) do not have such a mode. To acquire a sufficient data set to constrain the nine elastic constants, we prepared bar graphs showing the sensitivity of each elastic constant to three elastic wave modes in a crystallographic direction (Supplementary Figure 4). We can learn the strategy for the measurement sequence as shown in Supplementary Figure 5 according to three criteria: the sensitivity to the target elastic constant, relative intensity of the corresponding mode, and expected peak position. For example, cases A and B are ideal to determine C_{11} and C_{66}, respectively, while C and D are effective to constrain C_{12} and C_{31}, respectively. We made 3 or 4 measurements changing $\boldsymbol{dq}$ values for each Bragg diffraction spot.

Supplementary References

1. Kittel, C. *Introduction to Solid State Physics* (John Willey & Sons, Hoboken, 2004).

2. Royer, D. & Dienlesaint, E. *Elastic Waves in Solids I: Free and Guided Propagation* (Springer; Berlin, 2000).